



Journal of Advanced Research in Fluid Mechanics and Thermal Sciences

Journal homepage:
https://semarakilmu.com.my/journals/index.php/fluid_mechanics_thermal_sciences/index
ISSN: 2289-7879



Effectiveness of Cone Angle on Surface Pressure Distribution along Slant Length of a Cone at Hypersonic Mach Numbers

Javed Shoukat Shaikh¹, Khizar Ahmed Pathan², Krishna Kumar¹, Sher Afghan Khan^{3,*}

¹ Department of Applied Sciences and Humanities, MIT School of Engineering, MITADT University, Pune-412201, Maharashtra, India

² Department of Mechanical Engineering, Trinity College of Engineering and Research, Pune, India

³ Department of Mechanical Engineering, Faculty of Engineering, IIUM, Gombak Campus, Kuala Lumpur, Malaysia

ARTICLE INFO

Article history:

Received 8 December 2022

Received in revised form 20 February 2023

Accepted 27 February 2023

Available online 17 March 2023

Keywords:

Cone; hypersonic flow; surface pressure

ABSTRACT

In the present study, the prime attention is to numerically simulate the surface pressure distribution over the slant length of the cone at the various Mach numbers and for the considerable range of semi-cone angles. The Computational Fluid Dynamics (CFD) analysis is used to simulate the surface pressure distribution numerically. The hypersonic Mach numbers, semi-cone angle, and various locations along the slant length of a cone are considered parameters for this research work. The Mach numbers (M) considered for the research work are 5, 7, 9, 11, 13, and 15. The cone angle (θ) from 5° to 25° is considered. The results of pressure (P/P_∞) are recorded at various locations (x/L) along the slant length of the cone as 0.1 to 1. The pressure distribution results are obtained by CFD analysis and compared with the analytical results available in the literature for Mach number 5. The findings obtained by CFD analysis and analytical results show good agreement. In this investigation, it is observed that the Mach number, cone angle, and slant length of the cone are the highly influential parameters for the surface pressure distribution. The pressure distribution over the slant length of the cone increases with an increase in the Mach number and the semi-cone angle.

1. Introduction

The study of supersonic and hypersonic flow regimes is a complete and vital part of the domain of space investigation. Some of the crucial areas of research include space science, long-range weapons, and space vehicles. The concept similarity rule in the case of irrotational and unsteady hypersonic flow was first derived by Tisen [1]. It is applied to the large scale of Mach numbers. The results obtained by him show good agreement with the experimental results. The unsteady flow with high Mach numbers over a thin aerofoil was studied by Hayes [2]. The unsteady hypersonic flow using the tangent-wedge approximation method and shock expansion theory was studied by Zartarian *et al.*, [3]. Carrier [4] obtained the exact solution in the two-dimensional flow of an oscillating wedge when the shock wave is attached. Hui [5] studied and extract a solution that is used for all supersonic

* Corresponding author.

E-mail address: sakhan@iium.edu.my

<https://doi.org/10.37934/arfmts.104.1.185203>

Mach numbers and wedge angles constantly for the attached shock wave of an oscillating flat plate with a two-dimensional flow. Hui *et al.*, [6] studied the unsteady hypersonic flow in the case of a wedge when the shock wave is attached. Hui [5] studied and extract a solution that is used for all supersonic Mach numbers and wedge angles constantly for the attached shock wave of an oscillating flat plate with a two-dimensional flow. Hui *et al.*, [6] studied the unsteady hypersonic flow in the case of detached shock wave.

Oscillating delta wings with attached shock waves have been studied by Lui *et al.*, [7]. The concept of an oscillating airfoil in pitch at a wide range of Mach numbers and unsteady piston theory was revealed by Light Hill [8]. The large incidence two-dimensional hypersonic similitude and piston theory was developed by Ghosh *et al.*, [9]. It includes Light Hill's [8] piston theory and Mile's Shock expansion theory [10]. Ghosh [11] has applied this concept of order of ϕ^2 where ϕ is the angle between the plane approximating the windward surface and the attached shock wave. Ghosh [11] obtained the similitude for oscillating delta wings for attached shock waves at hypersonic Mach number with a high angle of incidence. The variation in surface pressure distribution at the large angle of incidence and high Mach numbers in the case of curved leading edge for the delta wing was studied by Crasta *et al.*, [12]. Musavir *et al.*, [13] studied the computational and analytical investigation of aerodynamic derivatives for the oscillating wedge. The CFD simulation with analytical and theoretical validation of various flow parameters for the wedge at supersonic Mach number was obtained by Khan *et al.*, [14]. Aerodynamic coefficients at Mach 6 for the blunt body in the idea of without and with a spike were studied by Kalimuthu *et al.*, [15]. The effect of trailing edge geometry on the aerodynamics of low-speed BWB aerial vehicles was studied by Zuhair *et al.*, [16]. Meng *et al.*, [17] studied the double-cone missile by the combined spike and multi-jet. Shaikh *et al.*, [18] studied the analytical computational analysis of pressure at the nose of a 2D wedge in high-speed flows. Ayesha Shabana *et al.*, [19] studied the stiffness and damping derivatives of an ogive in the limiting case of Mach number and specific heat ratio. Computational analysis of pressure distribution over a 2D wedge in the supersonic and hypersonic flow regimes is studied by Shaikh *et al.*, [20].

In the current investigation, the main objective is to obtain surface pressure distribution along the slant length of the cone. The CFD analysis results of pressure with various semi-cone angles and Mach number are obtained using ANSYS workbench. The CFD analysis along with the parametric study using ANSYS are used for analysis. The Mach numbers are considered as 5, 7, 9, 11,13 15, the semi-cone angles are considered from the range of 5° to 25° , and the location(x/L) along the slant length of the cone is 0.1 to 1. Figure 1 shows the geometry of a cone.

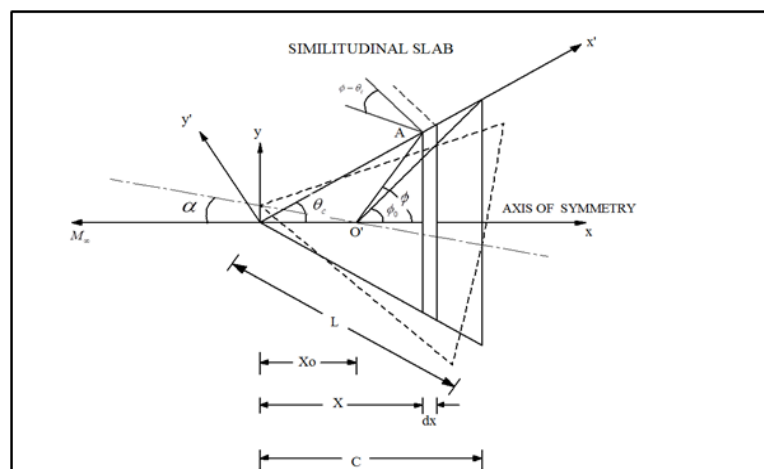


Fig. 1. Geometry of cone

The expression for pressure ratio at the nose of the cone in the case of bow-attached shock obtained by Ghosh [11] is given in Eq. (1).

$$\frac{P}{P_a} = 1 + \gamma M_p^2 \left(1 + \frac{1}{4} \varepsilon \right) \quad (1)$$

here, P is the pressure; P_a is the atmospheric pressure; M_p is piston Mach number of equivalent piston.

ε , the density ratio and given by Eq. (2).

$$\varepsilon = \frac{2 + (\gamma - 1)M_p^2}{2 + (\gamma + 1)M_p^2} \quad (2)$$

The piston Mach number is given by Eq. (3).

$$M_p = M_\infty \sin \theta_c \quad (3)$$

where θ_c is the semi-angle of the cone and M_∞ is the free stream Mach number.

In the case of an oscillating cone, Ghosh [11] is adopted the equilibrium surface of the cone is perpendicular to the similitude slab at a distance x^1 from the apex. The boat tail helmets can reduce drag studied by Pathan *et al.*, [21] and found that the aerodynamic drag reduces when the helmet shape is streamlined. Azami *et al.*, [22] explored the experimental research of wall pressure and the effect of microjet. The base pressure variation in external and internal flows using CFD analysis is studied by Pathan *et al.*, [23] and revealed that the internal and external suddenly expanded flows are nearly the same in the base region of the flow field. Khan *et al.*, [24] and Pathan *et al.*, [25-28] and Khan *et al.*, [29] have explored and studied the various methods to control base pressure. In suddenly expanded flows, the optimization of enlarged duct length was studied by Pathan *et al.*, [30].

Based on the literature, it has been found that the surface pressure along the slant length of the cone has not been studied. In the present research work, the variation of surface pressure distribution along the slant length of the cone has been obtained. It is done by applying various flow parameters for the cone to simulate the surface pressure along the slant length of the cone numerically by using Computational Fluid Dynamics (CFD) analysis. The numerical solution results so obtained for the surface pressure of the cone for the hypersonic Mach Numbers as 5, 7, 9, 11, 13, 15, the semi angles of the cone from angles (θ) are from 5° to 25° and for the location(x/L) from 0.1 to 1.0 along the slant length of the cone.

2. Methodology

2.1 CFD Analysis

For the analysis, the Computational Fluid Dynamics (CFD) analysis is applied using the Academic licensed ANSYS Workbench and Fluent. Using ANSYS workbench the meshing and modeling are completed and for the analysis and post-processing, ANSYS Fluent was used. To obtain the correct and precise numerical results, the structured mesh is used [31-43]. The Mach numbers span interval taken into the account as 5.0, 7.0, 9.0, 10.0, and 15.0 for the analysis together with semi-cone angles as 5° , 10° , 15° , 20° and 25° . The combination of all potential parameters is considered for CFD analysis for weak solutions where the shock wave is attached.

2.1.1 Modelling

All the axisymmetric geometries by varying the cone angle are modeled by using ANSYS design Modeler. The geometry of the cone and enclosure are shown in Figure 2. All the geometries are accounting for the different cone angles as 5°, 10°, 15°, 20° and 25°. The enclosure is created for CFD analysis with five times the length (L) on the top and bottom sides, three times the length (L) from the front side, and five times the length (L) from the backside.

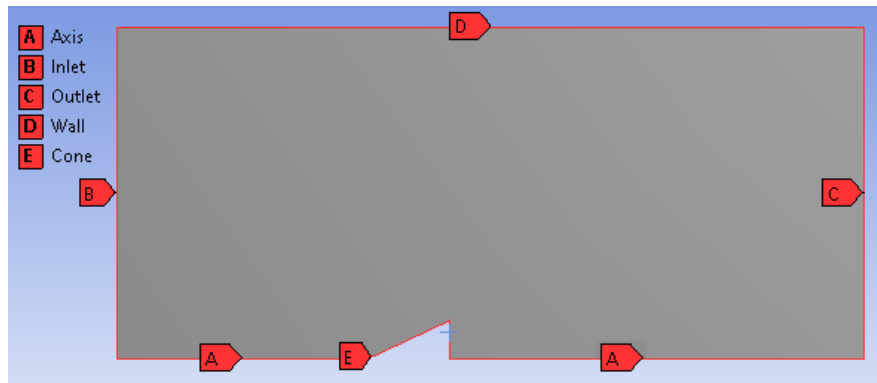


Fig. 2. Geometry of 2D axisymmetric cone and enclosure for CFD analysis

2.1.2 Meshing

To finalize the optimal mesh size, the grid independence test was performed before proceeding with the meshing. For the semi-cone angle of 15° and Mach number 9, the grid independence test was performed with mesh size from the range 0.25 mm to 15 mm.

Figure 3 exhibits the results of the grid independence test. The results clearly show that the results are stable for a mesh element size of 3 mm and the mesh element size of 3 mm can be taken into consideration for further CFD analysis. The mesh element size of 1 mm is adopted for better accuracy in subsequent CFD analysis.

Figure 4(a) reveals the 2D axisymmetric meshed model, and the expanded view of the cone geometry is shown in Figure 4(b). For the entire meshing, the Hexahedral dominant mesh scheme is adopted.

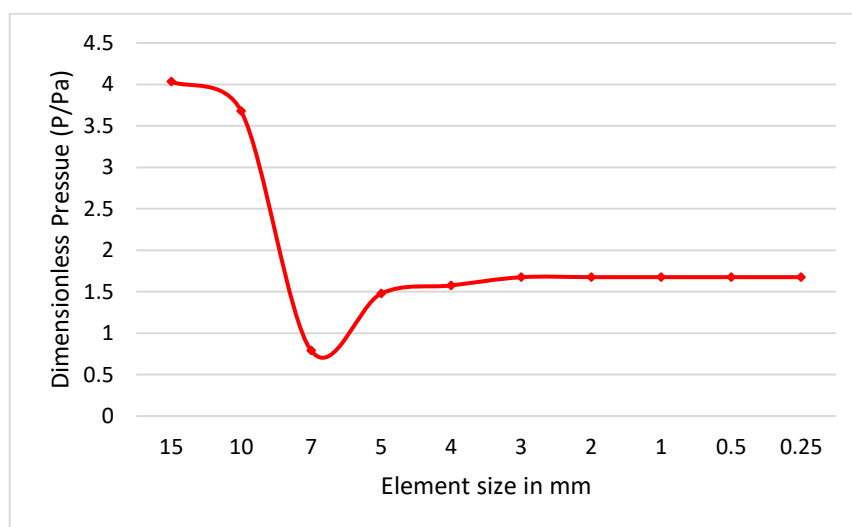


Fig. 3. Grid independence test

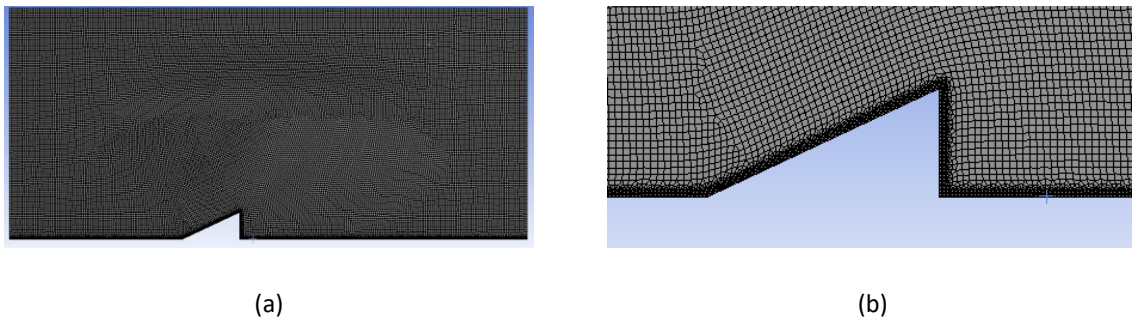


Fig. 4. 2D axisymmetric meshed model (a) Complete Geometry (b) Enlarged view of cone

2.1.3 CFD analysis

The complete CFD analysis is carried out by using the set of all feasible combinations of parameters. After setting the boundary conditions the solution is initialized and it runs for a minimum of 10000 iterations. In several cases, the solution is converged within 1000 iterations.

The most common k -epsilon turbulent model is used for the analysis. It involves two additional transport equations to show the turbulent properties of the flow. The velocity inlet and pressure outlet are specified to define inlet and outflow boundary conditions respectively. The inlet velocity is set by calculating the velocity according to the Mach number. At the outlet, the pressure is set to zero atmospheric pressure. The method of SIMPLE approach is applied while doing the analysis. The density-based problem solver is used for the analysis as the flow is compressible and hypersonic.

2.1.4 Validation of present work with literature

The results which are obtained from the CFD analysis are validated with the available results in the literature and displayed in Figure 5. Aysha Shabana *et al.*, [31] have studied and computed the pressure of an oscillating cone concerning piston Mach number = 5. Figure 5 indicates an overall agreement between the results of pressure variation by analytical study and the present research work.

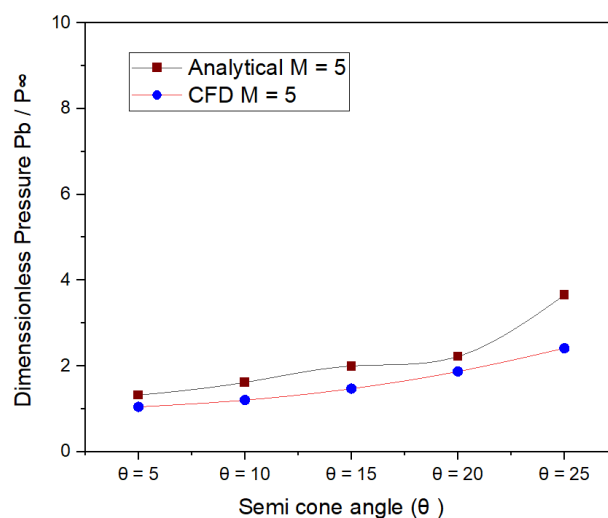
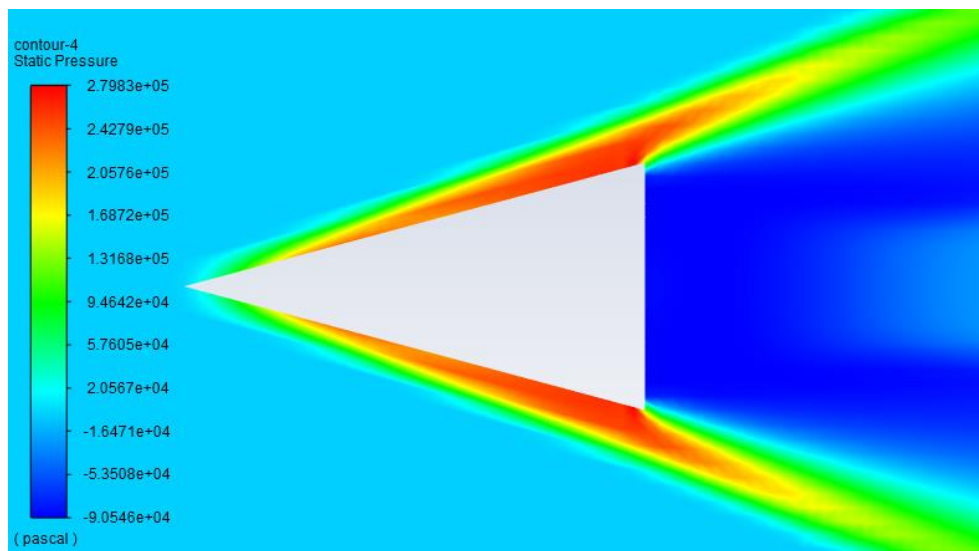


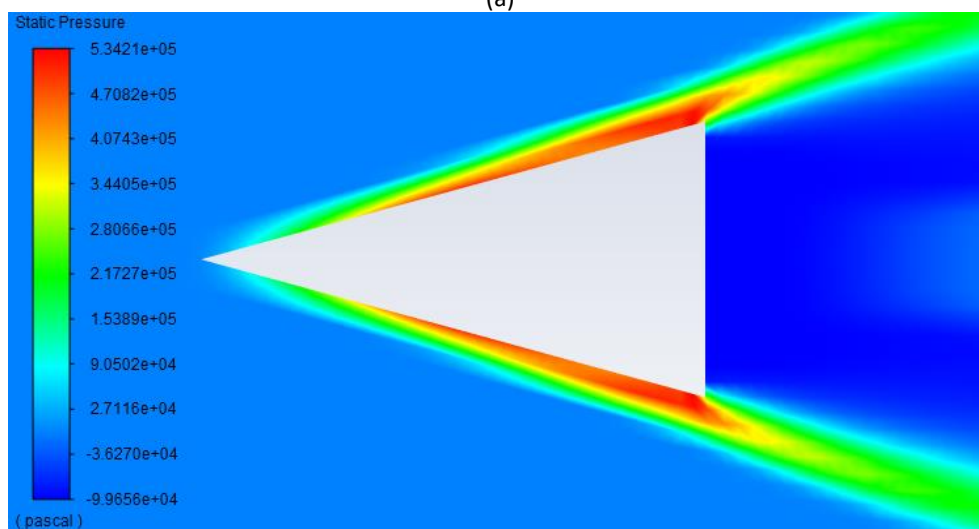
Fig. 5. Comparison of Variation of dimensionless pressure by the analytical study and by CFD at M = 5

2.2 Results of Pressure Contours

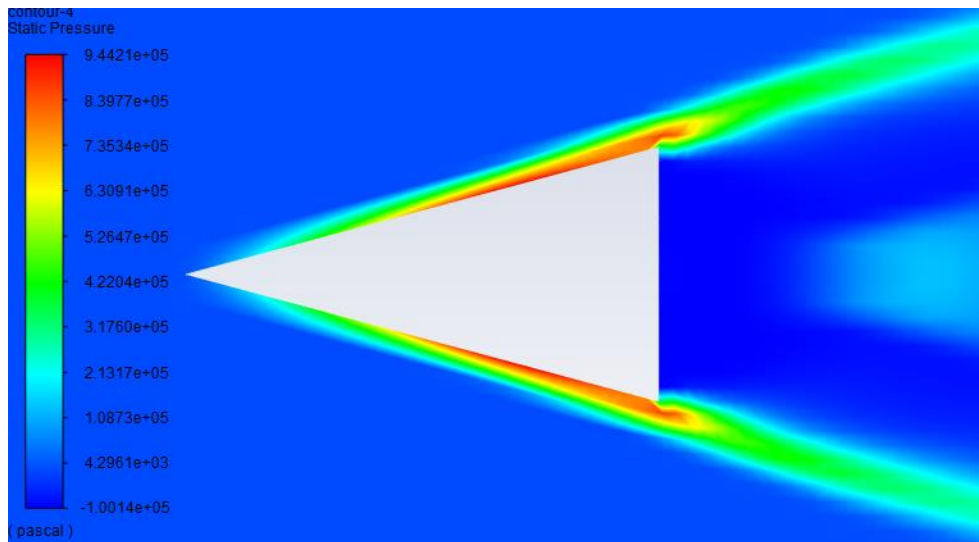
Figure 6 shows the pressure contours for various Mach numbers at the semi-cone angle of the cone as 15° . From the obtained results, it can be seen that the Mach cone angle reduces when the Mach number increases.



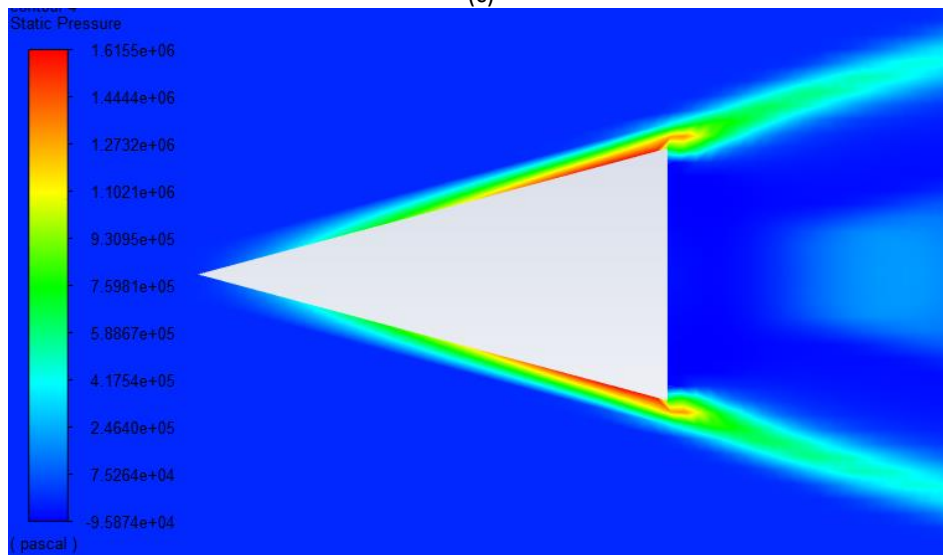
(a)



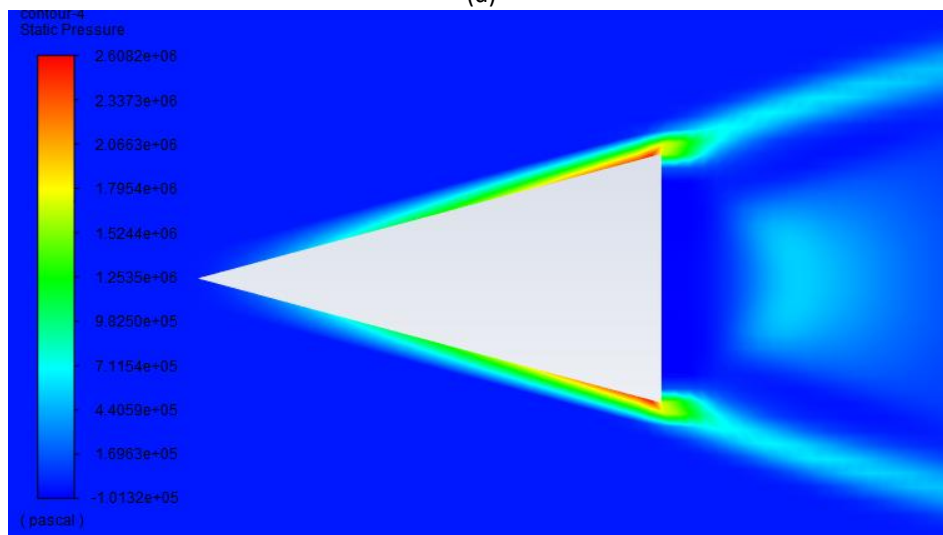
(b)



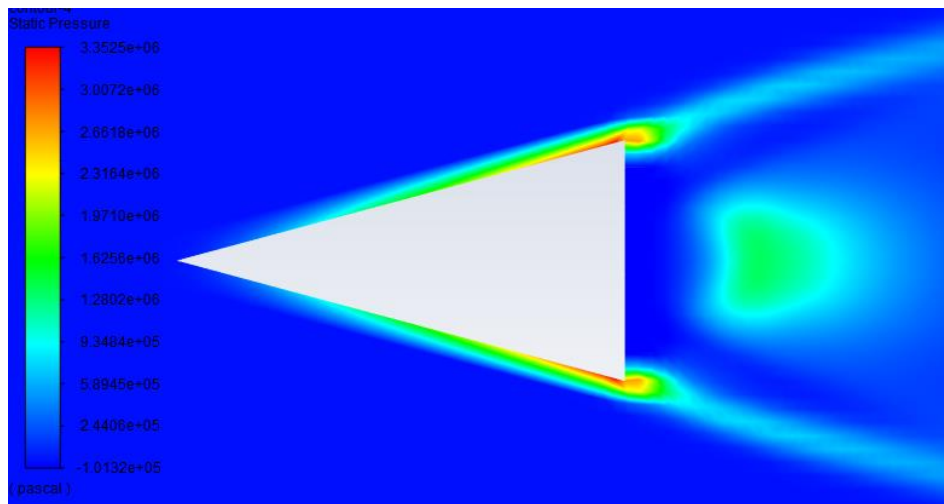
(c)



(d)



(e)



(f)

Fig. 6. Contours of static pressure for various Mach numbers at a semi-cone angle (θ) 15° (a) $M = 5$ (b) $M = 7$ (c) $M = 9$ (d) $M = 11$ (e) $M = 13$ (f) $M = 15$

3. Results and Discussion

3.1 Main Effects Mach Number Plots for Dimensionless Static Pressure

For all cases, the mean values of pressure are considered and plotted in Figure 7 which depicts the major effect of Mach number on dimensionless static pressure (P/P_a) i.e. the ratio of pressure at a point (P) to the atmospheric pressure (P_a) at the nose of the cone. From the obtained results, it is observed that the static pressure at the nose of the cone increases with an increase in Mach number.

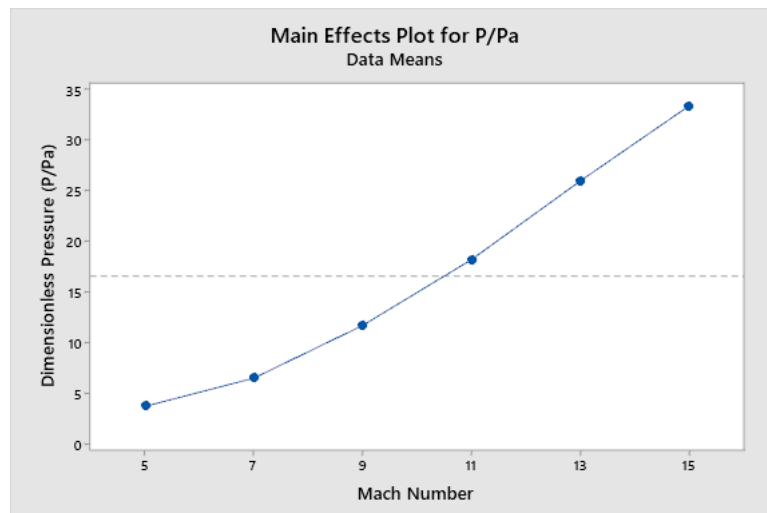


Fig. 7. Main effect of Mach number on pressure at the nose of the cone

3.2 Main Effects Semi Cone Angle Plots for Dimensionless Static Pressure

Figure 8 depicts the major effect of the semi-cone angle plot on dimensionless static pressure (P/P_a) at the nose of the cone. According to the obtained results, it is clear that as the semi-cone angle increases that leads to an increase in the static pressure at the nose of the cone.

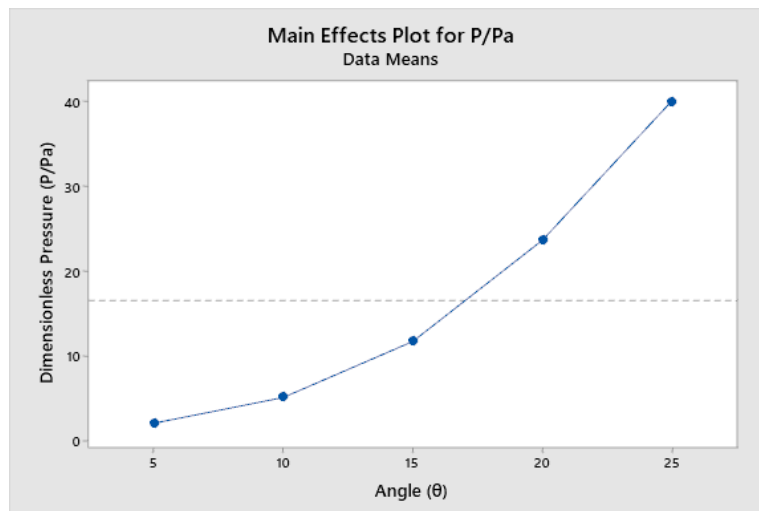


Fig. 8. Main effect of semi-cone angle on pressure at the nose of the cone

3.3 Main Effects of Location along Slant Length of the Cone for Dimensionless Static Pressure

Figure 9 shows the main effect of location (x/L) along the slant length of the cone plots for dimensionless static pressure. Based on the obtained results, the static pressure increases from the location 0.1 to till 0.9. After location 0.9 the pressure leads to a drop from location 0.9 to 1.0.

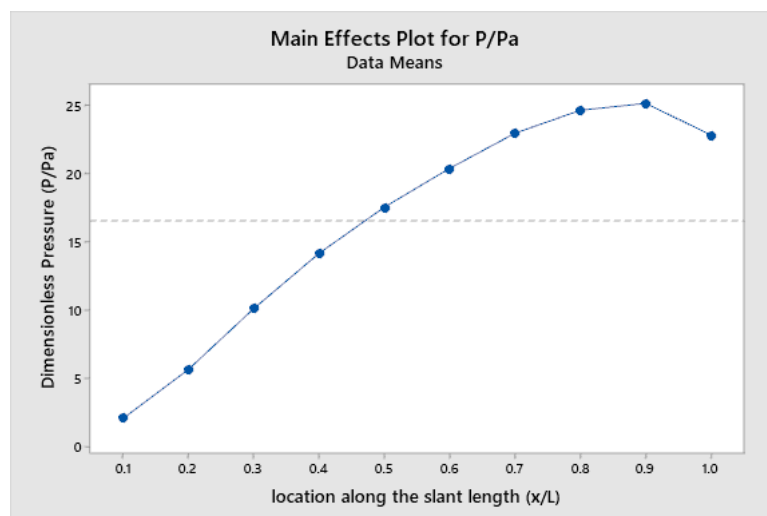


Fig. 9. Main effect of location along the slant length of the cone on pressure at the nose of the cone

3.4 Surface Pressure at Various Locations along the Length of the Cone for a Constant Mach Number.

At a constant Mach number, the CFD analysis results for the pressure over the fraction of the slant length of the cone (x/L) have been obtained from the ANSYS software, and the graphs are plotted. The dimensionless pressure values are so obtained by dividing the static pressure values by atmospheric pressure.

Figure 10 depicts the change in dimensionless static pressure vs location (x/L) along the slant length of the cone at constant Mach number $M = 5$ for various semi-cone angles. The results clearly show that there is a continuous increase in the pressure as the semi-cone angle increases. Also, for

all the semi-cone angles, the pressure increases from the location 0.1 to 0.3. The pressure decreases from the location 0.3 onwards to 0.6. It is also observed the marginal changes in pressure after the location is 0.6 to 1.0 for all the values of semi cone angle.

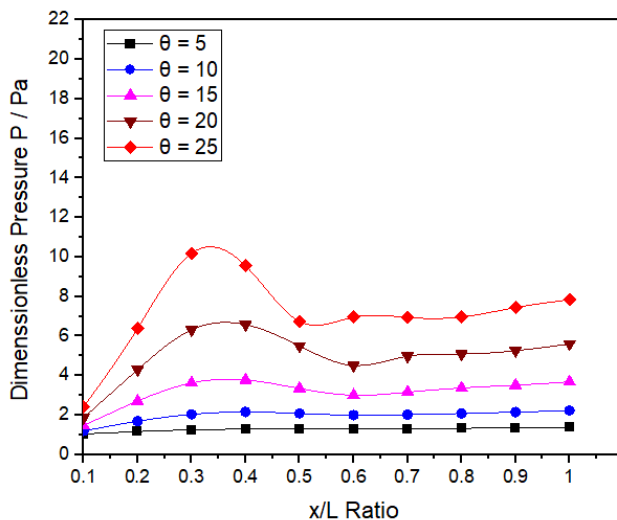


Fig. 10. Variation of dimensionless pressure along the slant length (x/L) at M = 5

Figure 11 reveals the variation in dimensionless static pressure Vs. location (x/L) along the slant length of the cone at a constant Mach number M = 7 for various semi-cone angles. From the results, it is observed that, as the semi-cone angle increase, there is an increase in pressure. It is also seen that the pressure increases from the location 0.1 to 0.5 for all the semi-cone angles. The pressure decreases from the location 0.5 onwards to 0.7. The marginal variation is observed in the pressure after the location 0.7 to 1.0 for all the values of the semi-cone angle.

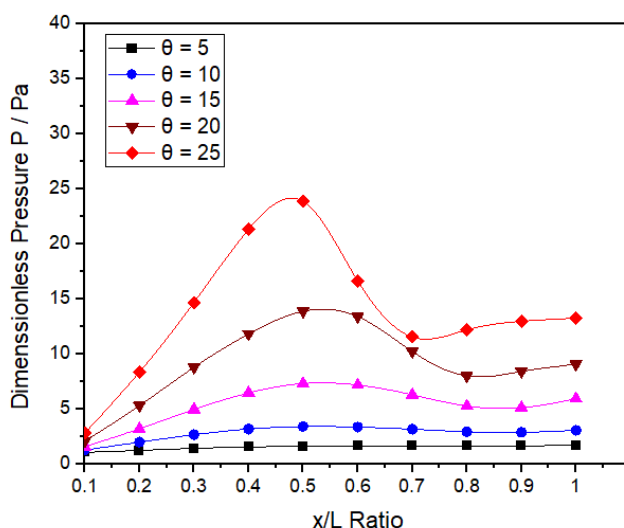


Fig. 11. Variation of dimensionless pressure along the slant length (x/L) at M = 7

Figure 12 displays the variation in dimensionless static pressure Vs. location(x/L) along the slant length of the cone at constant Mach number M = 9 for various semi-cone angles. From the results, it is observed that there is an increase in the pressure continuously along the slant length of the cone

for all semi-cone angles of the cone. It is also observed that the pressure increases from the location 0.1 to 0.7 for all values of the semi-cone angle. Further, the pressure decreases from a location of 0.7 to 0.9. A slight variation is observed in pressure between the locations 0.9 to 1.0 for all the values of semi-cone angles.

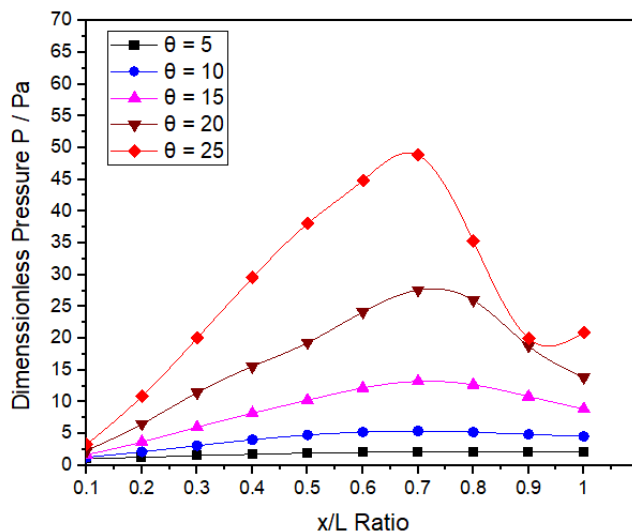


Fig. 12. Variation of dimensionless pressure along the slant length (x/L) at $M = 9$

Figure 13 displays the variation in dimensionless static pressure Vs. location (x/L) along the slant length of the cone at constant Mach number $M = 11$ for various semi-cone angles. From the results, it is observed that there is an increase in pressure continuously along the length of the cone for all the values of the semi-cone angle. It is also observed that the pressure increases from the location 0.1 to till 0.9 for the semi-cone angles ranging from 5° to 20° . For a semi-cone angle of 25° the pressure increases from location 0.1 to till 0.8 and then the pressure decreases rapidly from a location 0.7 to 1.0. A slight variation is observed in pressure between the locations 0.9 and 1.0 for the semi-cone angle from 5° to 20° .

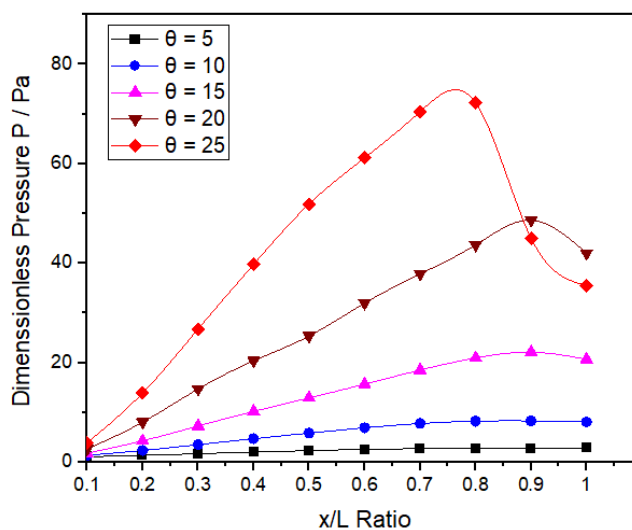


Fig. 13. Variation of dimensionless pressure along the slant length (x/L) at $M = 11$

Figure 14 depicts the change in dimensionless static pressure Vs. location(x/L) along the slant length of the cone at constant Mach number $M = 13$ for various semi-cone angles. The results clearly show that there is a continuous increase in pressure along the slant length of the cone for all semi-cone angles of the cone. It is also observed that the pressure increases from a location 0.1 to 1.0 for the semi-cone angles ranging between 5° to 20° . For the semi-cone angle of 25° the pressure increases from a location 0.1 to till 0.9 and the pressure decreases rapidly from a location 0.9 to 1.0. The marginal change in pressure is observed between the locations 0.9 to 1.0 for the angles of incidence 5° to 20° .

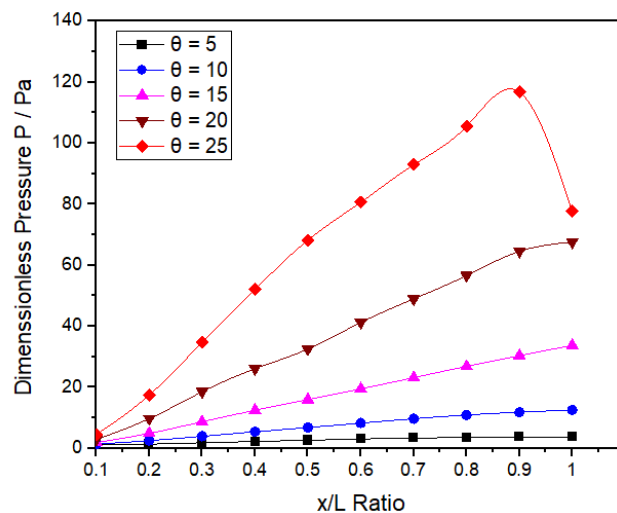


Fig. 14. Variation of dimensionless pressure along the slant length (x/L) at $M = 13$

Figure 15 shows the variation in dimensionless static pressure Vs. location (x/L) along the slant length of the cone at constant Mach number $M = 15$ for various semi-cone angles. The results reveal that there is a continuous increase in pressure along the length of the cone for all semi-cone angles of the cone. It is also observed that the pressure increases from the location 0.1 to 1 for the semi-cone angles 5° to 20° . For a semi-cone angle of 25° the pressure increases from location 0.1 to till 0.9 and the pressure decreases suddenly from a location 0.9 to 1.0.

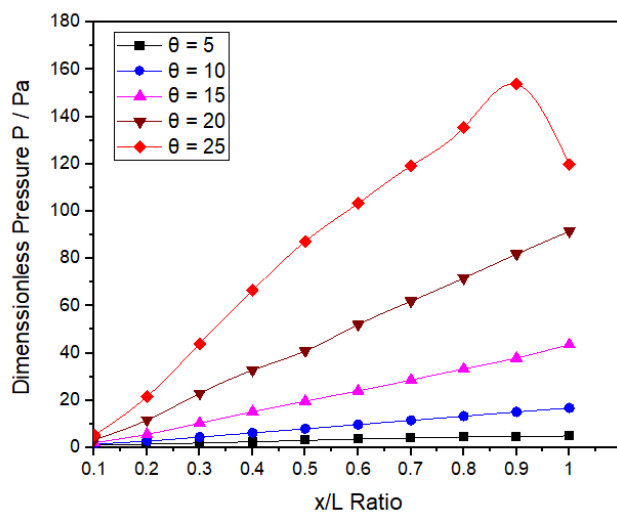


Fig. 15. Variation of dimensionless pressure along the slant length (x/L) at $M = 15$

3.5 Surface Pressure at Various Locations along the Slant Length of the Cone at a Constant Semi-Cone Angle

At a constant semi-cone angle, the CFD analysis results for the pressure over the various location along the slant length (x/L) of the cone have been obtained from the ANSYS software. The dimensionless pressure values are so obtained by dividing the static pressure by atmospheric pressure.

Figure 16 shows the variations in dimensionless static pressure Vs. location(x/L) along the slant length of the cone at constant semi-cone angle $\theta = 5^\circ$ for various Mach numbers. The results reveal that there is a continuous increase in pressure along the slant length of the cone from the location 0.1 to 0.3 for all the Mach numbers. It is also observed that the variation in pressure is significant for Mach numbers 13 and 15 at each location along the slant length of the cone. For the Mach numbers 5, 7, 9, and 11 marginal variations are observed in the pressure along the slant length of the cone from the location 0.5 to 1.0.

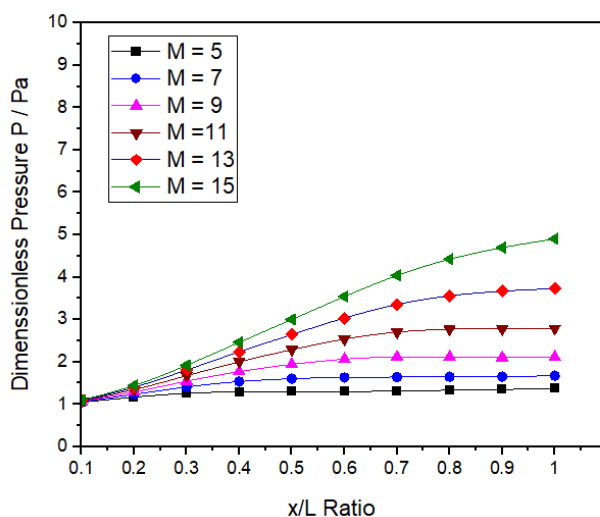


Fig. 16 Variation of dimensionless pressure along the slant length (x/L) at $\theta = 5^\circ$

Figure 17 displays the changes in dimensionless static pressure Vs. location (x/L) along the slant length of the cone at constant semi-cone angle $\theta = 10^\circ$ for various Mach numbers. From the results, it is clear that there is a continuous rise in pressure along the slant length of the cone from 0.1 to 0.3 for all the Mach numbers. It is also seen that the variation in pressure is significant for Mach numbers 13 and 15 at each location along the slant length of the cone. For the Mach numbers 5, 7, 9, and 11 marginal variations are observed in the pressure along the slant length of the cone from the location 0.6 to 1.0.

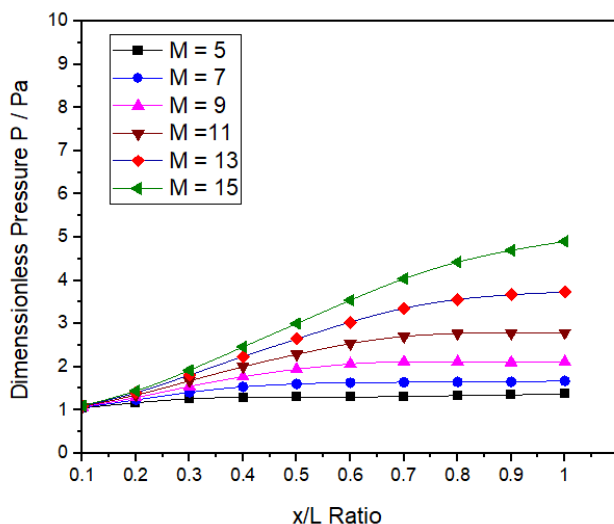


Fig. 17. Variation of dimensionless pressure along the slant length (x/L) at $\theta = 10^\circ$

Figure 18 shows the variations in dimensionless static pressure Vs. location (x/L) along the slant length of the cone at constant semi-cone angle $\theta = 15^\circ$ for various Mach numbers. From the results, it is clear that there is a continuous rise in pressure at the location from 0.1 to 0.3 along the slant length of the cone for all the Mach numbers. It is also observed that the variation in pressure is significant for the Mach numbers 11, 13, and 15 at each location along the slant length of the cone. For the Mach numbers, 5, 7, and 9 marginal variations in pressure are observed along the slant length of the cone from the location 0.5 to 1.0.

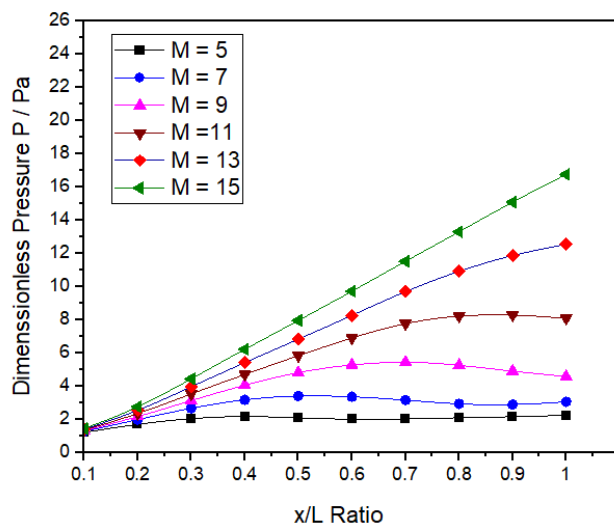


Fig. 18. Variation of dimensionless pressure along the slant length (x/L) at $\theta = 15^\circ$

Figure 19 reveals the variations in dimensionless static pressure Vs. location (x/L) along the slant length of the cone at constant semi-cone angle $\theta = 20^\circ$ for various Mach numbers. The results clearly show the continuous increase in pressure along the slant length of the cone for all the Mach numbers from the location 0.1 to 0.3. It is also observed that the variation in pressure is significant for the Mach numbers 11, 13, and 15 at each location along the slant length of the cone. For the Mach numbers 5, 7, and 9 marginal variations are observed in the pressure along the slant length of the cone from the location 0.5 to 1.0.

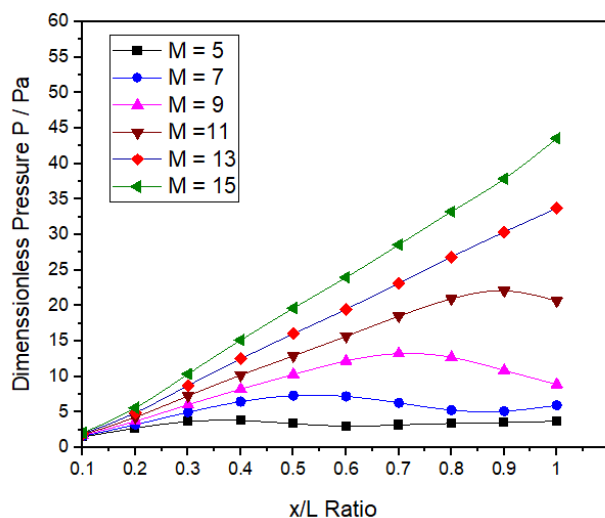


Fig. 19. Variation of dimensionless pressure along the slant length (x/L) at $\theta = 20^\circ$

Figure 20 reveals the variations in dimensionless static pressure Vs. location(x/L) along the slant length of the cone at constant semi-cone angle $\theta = 25^\circ$ for various Mach numbers. The results clearly show the continuous rise along the slant length of the cone for all the Mach numbers from the location 0.1 to 0.3. For Mach numbers 9 and 11, the change in pressure is significant from a location of 0.1 to 0.7 and pressure gets fluctuated from a location of 0.7 to 1. For Mach numbers 13 and 15, the change in pressure is significant from the location 0.1 to 0.9 and pressure is reduced from the location 0.9 to 1.0.

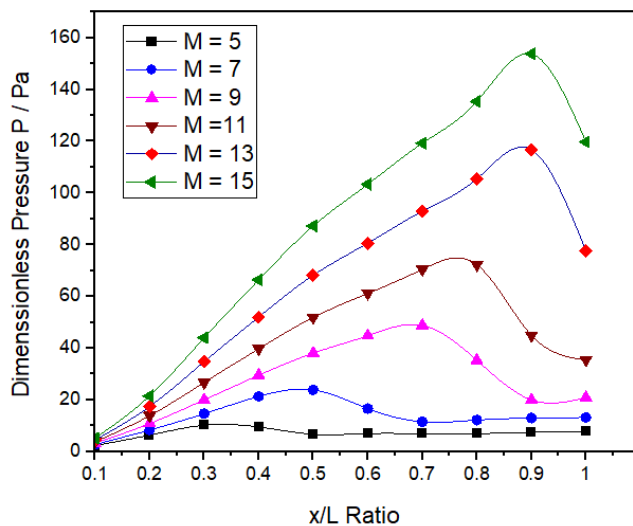


Fig. 20. Variation of dimensionless pressure along the slant length (x/L) at $\theta = 25^\circ$

3.6 The Contour Plot of Dimensionless Pressure Vs Mach Number and Semi-Cone Angle

The contour plot for the dimensionless pressure at the nose of the cone for all the Mach numbers and semi-cone angles is shown in Figure 21. It can be observed that the pressure on the nose of the cone increases with an increase in the semi-cone angle and Mach number.

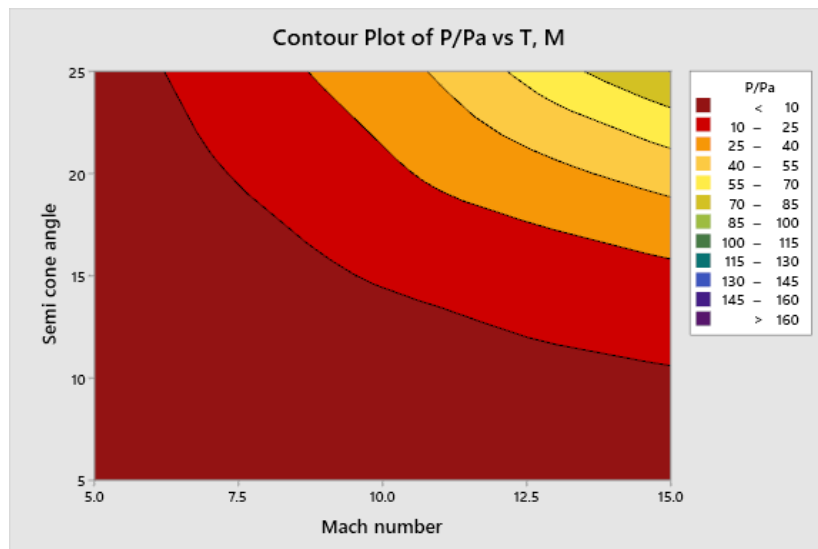


Fig. 21. Variation of Dimensionless Pressure Vs Mach number and semi-cone angle

3.7 The Contour Plot of Dimensionless Pressure Vs Mach Number and Location along the Slant Length of the Cone Length

The contour plot for the dimensionless pressure at the nose of the cone for all the Mach numbers and locations along the slant length of the cone is shown in Figure 22. It can be observed that the pressure along the slant length of the cone initially increases with an increase and then reduces. The pressure values along the slant length are higher than the pressure values on the nose.

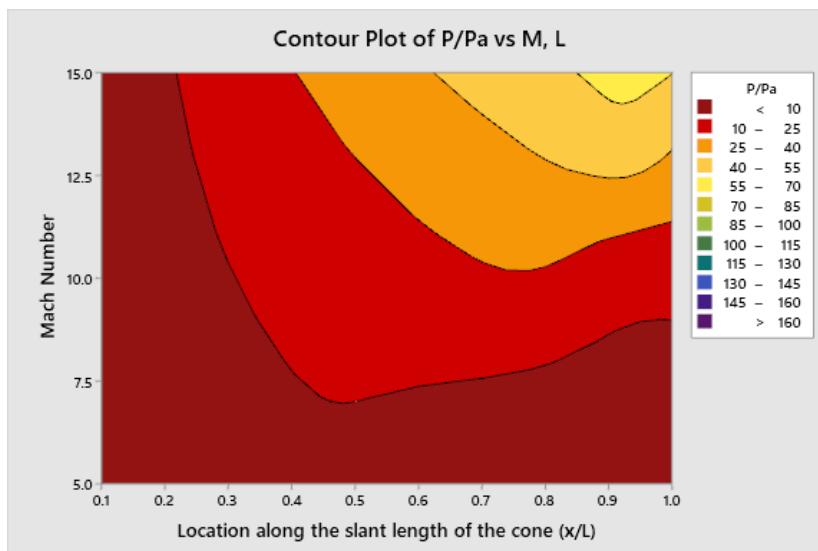


Fig. 22. Variation of Dimensionless Pressure Vs Mach number and location along the slant length of the cone

4. Conclusions

The above research work demonstrates its wide range of applications in the field of defense and aerospace applications for parameters like Mach number, semi-cone angle, and slant length of the cone. Based on the above results it can be concluded that the static pressure increases with the

increase in Mach numbers and the semi-cone angle of the cone. It is also observed that both Mach number and semi-cone angle are the influential parameters on the variation of surface pressure. It has been found that for the Mach numbers, 5 and 7 with the semi-cone angles 5 and 10 degrees, the variation in surface pressure is marginal and for the Mach numbers 9, 11, 13, and 15 with the angle of incidence 15°, 20° and 25° the pressure value increases up to the certain length. The results obtained by CFD analysis and the analytical results present in the literature show excellent agreement. The present investigation gives good results with prominent computational ease. These findings are beneficial in the designing stage of aerospace vehicles as the cost involved in the wind tunnel test is very high. Hence, in the initial development, these results can be used to improve the design of the aerospace vehicle.

Acknowledgment

The authors received no specific funding for this study.

References

- [1] Tsien, Hsue-Shen. "Similarity laws of hypersonic flows." *Journal of Mathematics and Physics* 25, no. 1-4 (1946): 247-251. <https://doi.org/10.1002/sapm1946251247>.
- [2] Hayes, W. D. "On hypersonic similitude." *Quart. Appl. Math.* 5 no. 1 (1947): 105-106. <https://doi.org/10.1090/qam/20904>.
- [3] Zartarian, G., Hsu, P. T., Ashley, H. "Dynamic air loads and aeroelastic problems at entry Mach numbers." *Journal of the Aerospace Science* 28, no. 3, (1961): 209-222. <https://doi.org/10.2514/8.8927>.
- [4] Carrier, G. F. "The oscillating wedge in the supersonic stream." *Journal of Aeronautical Sciences* 16, no. 3 (1949): 150-152. <https://doi.org/10.2514/8.11755>.
- [5] Hui, W.H. "Supersonic and hypersonic flow with attached shock waves over delta wings." *Proc. Roy. Soc. London. A. Math. Phys. Sci.* 325, 1561, (1971): 251-268. <https://doi.org/10.1098/rspa.1971.0168>.
- [6] Hui, W. H., Hemdan, H. T. "Unsteady hypersonic flow over delta wings with detached shock waves." *American Institute of Aeronautics and Astronautics Journal* 14, no. 4 (1976): 505-511. <https://doi.org/10.2514/3.7120>.
- [7] Liu, D. D., and W. H. Hui. "Oscillating delta wings with attached shock waves." *AIAA Journal* 15, no. 6 (1977): 804-812. <https://doi.org/10.2514/3.7371>.
- [8] Lighthill, M.J. "Oscillating aerofoil at high Mach numbers." *J. Aeronaut. Sci.* 20, no. 6 (1953): 402-406. <https://doi.org/10.2514/8.2657>.
- [9] Ghosh, K. and Mistry, B.K. "Large incidence hypersonic similitude and oscillating non-planar wedges." *AIAA J* 18, no. 8 (1980): 1004-1006. <https://doi.org/10.2514/3.7702>.
- [10] Miles, JOHN W. "Unsteady flow at hypersonic speeds, Hypersonic flow." *Butter worths Scientific Publications, London* (1960): 185-197.
- [11] Ghosh, K. "Hypersonic large deflection similitude for oscillating delta wings." *Aeronaut. J.* 88, no. 878 (1984): 357-361. <https://doi.org/10.1017/S0001924000020868>.
- [12] Crasta, Asha, S. Pavitra, and Sher Afghan Khan. "Estimation of surface pressure distribution on a delta wing with curved leading edges in hypersonic/supersonic flow." *International Journal of Energy, Environment and Economics* 24, no. 1 (2016): 67-73.
- [13] Musavir, B., Khan, S. A., Azam, Q., Janvekar, A. A. "Computational and analytical investigation of aerodynamic derivatives of similitude delta wing model at hypersonic speeds." *International Journal of Technology* 8, no. 3 (2017): 366-375. <https://doi.org/10.14716/ijtech.v8i3.6319>.
- [14] Khan, Sher Afghan, Abdul Aabid, and C. Ahamed Saleel. "CFD simulation with analytical and theoretical validation of different flow parameters for the wedge at supersonic Mach number." *International Journal of Mechanical and Mechatronics Engineering* 1 (2019).
- [15] Kalimuthu, R., R. C. Mehta, and E. Rathakrishnan. "Measured aerodynamic coefficients of without and with spiked blunt body at Mach 6." *Advances in aircraft and spacecraft science* 6, no. 3 (2019): 225-238. <https://doi.org/10.12989/aas.2019.6.3.225>.
- [16] Zuhair, Mohammed A. Ba, and A. Mohammed. "Trailing edge geometry effect on the aerodynamics of low-speed BWB aerial vehicles." *Advances in aircraft and spacecraft science* 6, no. 4 (2019): 283. <https://doi.org/10.12989/aas.2019.6.4.283>.

- [17] Meng, Y., Yan, L., Huang, W., Chen, J., Jie, L. "Coupled investigation on drag reduction and thermal protection mechanism of a double-cone missile by the combined spike and multi-jet." *Aerospace Science and Technology* 115, no. 1 (2021): <https://doi.org/10.1016/j.ast.2021.106840>.
- [18] Shaikh, Javed S., Krishna Kumar, Khizar A. Pathan, and Sher A. Khan. "Analytical and computational analysis of pressure at the nose of a 2D wedge in high speed flow." *Advances in aircraft and spacecraft science* 9, no. 2 (2022): 119-130. <https://doi.org/10.12989/aas.2022.9.2.119>.
- [19] Aysha Shabana., Asha Crasta., S.A.Khan., Abdul Aabid., Muneer Baig. "Computation of stiffness and damping derivatives of an ogive in a limiting case of Mach number and specific heat ratio." *Fluid Dynamics & Materials Processing* 19, no. 5 (2022): 1249-1267. <https://doi.org.10.32604/fdmp.2023.023158>.
- [20] Javed S. Shaikh, Krishna Kumar, Khizar A Pathan, and Sher A. Khan. "Computational analysis of surface pressure distribution over a 2d wedge in the supersonic and hypersonic flow regimes." *Fluid Dynamics & Materials Processing* 19, no. 6 (2023): 1637-1653. <https://doi.org/10.32604/fdmp.2023.025113>
- [21] Pathan K A, Khan S A, Shaikh A N, Pathan A A, and Khan S A. "An investigation of the boat-tail helmet to reduce drag." *Adv. Aircraft Spacecraft Sci.* 8, no. 1 (2021), 239- 250. <https://doi.org/10.12989/aas.2021.8.3.239>.
- [22] Azami, M. H., Faheem, M., Aabid, A., Mokashi, I., Khan, S. A. (2019). "Experimental research of wall pressure distribution and effect of the microjet at Mach 1.5." *International Journal of Recent Technology and Engineering* 8, no. 3 (2019): 1000–1003. <https://doi.org.10.35940/ijrte.B1187.0782S319>.
- [23] Pathan, Khizar Ahmed, Prakash S. Dabeer, and Sher Afghan Khan. "Investigation of base pressure variations in internal and external suddenly expanded flows using CFD analysis." *CFD Letters* 11, no. 4 (2019): 32-40.
- [24] Khan, Sher Afghan, and E. Rathakrishnan. "Active control of base pressure in supersonic regime." *Journal of Aerospace Engineering, Institution of Engineers, India* 87 (2006): 1-8.
- [25] Pathan Khizar Ahmed, S A Khan, and P S Dabeer. "An Investigation of Effect of Control Jets Location and Blowing Pressure Ratio to Control Base Pressure in Suddenly Expanded Flows." *Journal of Thermal Engineering* 6, no. 2 (2020): 15-23. <https://doi.org/10.18186/thermal.726106>.
- [26] Pathan, Khizar Ahmed, Syed Ashfaq, Prakash S. Dabeer, and Sher Afgan Khan. "Analysis of parameters affecting thrust and base pressure in suddenly expanded flow from nozzle." (2019).
- [27] Pathan, Khizar Ahmed, Prakash S. Dabeer, and Sher Afghan Khan. "Influence of expansion level on base pressure and reattachment length." *CFD Letters* 11, no. 5 (2019): 22-36.
- [28] Pathan, Khizar Ahmed, Prakash S Dabeer, and Sher Afghan Khan. "Effect of nozzle pressure ratio and control jet location to control base pressure in suddenly expanded flows." *Journal of Applied Fluid Mechanics* 12, no. 4 (2019): 1127-1135. <https://doi.org/10.29252/jafm.13.02.30049>.
- [29] Khan, A., Mazlan, N. M., Ismail, M. A. (2019). "Analysis of flow through a convergent nozzle at sonic Mach number for area ratio 4." *Journal of Advanced Research in Fluid Mechanics and Thermal Sciences* 62, no. 1 (2019): 66–79.
- [30] Pathan, Khizar A, Prakash S Dabeer, and Sher A Khan. "Enlarge duct length optimization for suddenly expanded flows." *Advances in Aircraft and Spacecraft Science* 7, no. 3 (2020): 203-214. <https://doi.org/10.12989/aas.2020.7.3.203>.
- [31] Sher Afghan Khan, M A Fatepurwala, K N Pathan, P S Dabeer & Maughal Ahmed Ali Baig. "CFD Analysis of Human Powered Submarine to Minimize Drag." *International Journal of Mechanical and Production Engineering Research and Development (IJMPERD)* 8, no. 3 (2018): 1057-1066. <https://doi.org/10.24247/ijmperdjun2018111>
- [32] Pathan, Khizar Ahmed, Prakash S Dabeer, and Sher Afghan Khan. "An investigation to control base pressure in suddenly expanded flows." *International Review of Aerospace Engineering* 11, no. 4 (2018): 162-169. <https://doi.org/10.15866/irease.v11i4.14675>.
- [33] Pathan, Khizar Ahmed, Prakash S Dabeer, and Sher Afghan Khan. "Optimization of area ratio and thrust in suddenly expanded flow at supersonic Mach numbers." *Case studies in thermal engineering* 12, (2018): 696-700. <https://doi.org/10.1016/j.csite.2018.09.006>.
- [34] Pathan Khizar Ahmed, S A Khan, and P S Dabeer. "CFD analysis of the effect of flow and geometry parameters on thrust force created by flow from nozzle." *2nd International Conference for Convergence in Technology (I2CT)*, (2017): 1121-1125. <https://doi.org/10.1109/I2CT.2017.8226302>.
- [35] Pathan Khizar Ahmed, S A Khan, and P S Dabeer. "CFD analysis of the effect of area ratio on suddenly expanded flows." *2nd International Conference for Convergence in Technology (I2CT)*, (2017): 1192-1198. <https://doi.org/10.1109/I2CT.2017.8226315>.
- [36] Pathan Khizar Ahmed, P S Dabeer, and S A Khan. "CFD analysis of the effect of Mach number, area ratio, and nozzle pressure ratio on velocity for suddenly expanded flows." *2nd International Conference for Convergence in Technology (I2CT)*, (2017): 1104-1110. <https://doi.org/10.1109/I2CT.2017.8226299>.
- [37] Shaikh, Sohail Khalil, Khizar Ahmed Pathan, Zakir Ilahi Chaudhary, B. G. Maripalle, and Sher Afghan Khan. "An Investigation of Three-Way Catalytic Converter for Various Inlet Cone Angles Using CFD." *CFD Letters* 12, no. 9 (2020): 76-90. <https://doi.org/10.37934/cfdl.12.9.7690>

- [38] Shaikh, Sohel Khalil, Khizar Ahmed Pathan, Zakir Ilahi Chaudhary, and Sher Afghan Khan. "CFD analysis of an automobile catalytic converter to obtain flow uniformity and to minimize pressure drop across the monolith." *CFD Letters* 12, no. 9 (2020): 116-128. <https://doi.org/10.37934/cfdl.12.9.116128>
- [39] Shamitha, Asha Crasta, Khizar Ahmed Pathan, Sher Afghan Khan. "Numerical simulation of surface pressure of a wedge at supersonic Mach numbers and application of design of experiments." *Journal of advanced research in applied mechanics* 101, no. 1, (2023): 1-18. <https://doi.org/10.37934/aram.101.1.118>
- [40] Shamitha, Asha Crasta, Khizar Ahmed Pathan, Sher Afghan Khan. "Analytical and Numerical Simulation of Surface Pressure of an Oscillating Wedge at Hypersonic Mach Numbers and Application of Taguchi's Method." *Journal of Advanced Research in Applied Sciences and Engineering Technology* 30, no. 1, (2023): 15-30. <https://doi.org/10.37934/araset.30.1.1530>
- [41] Osamah Othman Kanaani, Sami Abdelrahman Musa Yagoub, Shabir Habib, Akmal Aulia, Bonavian Hasiholan. "Prediction of Gas Coning in Hydrocarbon Reservoir using tNavigator." *Progress in Energy and Environment* 18, (2021): 1-22. <https://doi.org/10.37934/progee.18.1.122>
- [42] Mohamed Nazer, Muhammad Fadzrul Hafidz Rostam, Se Yong A/L Eh Noum, Mohammad Taghi Hajibeigy, Kamyar Shameli. "Performance analysis of photovoltaic passive heat storage system with microencapsulated paraffin wax for a thermoelectric generation." *Journal of Research in Nanoscience and Nanotechnology* 1, no. 1, (2021): 75-90. <https://doi.org/10.37934/jrnn.1.1.7590>
- [43] Elfaghi, Abdulhafid MA, Alhadi A. Abosbaia, Munir FA Alkbir, and Abdoulhdi AB Omran. "CFD Simulation of Forced Convection Heat Transfer Enhancement in Pipe Using Al₂O₃/Water Nanofluid." *Journal of Advanced Research in Numerical Heat Transfer* 8, no. 1 (2022): 44-49. <https://doi.org/10.37934/cfdl.14.9.118124>